Mining soil databases for landscape-scale patterns in the abundance and size distribution of hillslope rock fragments

Jill A. Marshall* and Leonard S. Sklar
Department of Geosciences, San Francisco State University, San Francisco, CA USA

*Correspondence to: Jill A. Marshall, Department of Geological Sciences, 325a Cascade Hall, University of Oregon, Eugene, OR 97403–1272, USA.
E-mail: jillm@uoregon.edu

ESPL

Earth Surface Processes and Landforms

ABSTRACT: Landscape-scale variation in rock fragments on soil-mantled hillslopes is poorly understood, despite the potential importance of rock fragments in soil weathering and coarse sediment supply to river networks. We explored the utility of soil survey databases for data mining, with the goals of identifying landscape-scale patterns in the abundance and size distribution of rock fragments (diameter $D > 2$ mm) and potential controls on grain size production. We focus on data from three regions: the Hawaiian Islands, and the Sierra Nevada and Cascade Mountains, where elevation transects span a range of environmental conditions. We selected pedons from pits dug on hillslopes with active soil production and transport. For the 27 pedons selected, we constructed depth-averaged grain size distributions and calculated the mass fraction of rock fragments (F_{RF}) and the median rock fragment grain size (D_{50RF}). We also categorized as bimodal, size distributions with a clear 'breakpoint' between fine and coarse modes. Several strong patterns emerge from the data. We find rock fragments in 85% of the pedons, primarily in distinct coarse modes within bimodal size distributions. Values of F_{RF} and D_{50RF} are strongly correlated, although the best-fit power law scaling between F_{RF} and D_{50RF} differs between the warmer Hawaiian, and colder Sierra Nevada and Cascade Mountain sites. We also find a regional contrast in the variation in F_{RF} with elevation; F_{RF} declines with elevation in Hawaii, but increases in the mainland sites. Although this contrast could be an artifact of variable lithology, precipitation may influence many patterns in the data. Lower mean-annual precipitation correlates with higher F_{RF}, dominantly bimodal distributions and surface enrichment in the vertical distribution of rock fragments. These observations may be useful in refining models of coarse sediment supply to rivers, and suggest opportunities for future work to test mechanistic hypotheses for rock fragment production on soil-mantled hillslopes. Copyright © 2011 John Wiley & Sons, Ltd.

KEYWORDS: soil; rock fragments; grain size distribution; bimodal; data mining; Critical Zone

Introduction

The abundance and size distribution of coarse particles in river channel sediments and hillslope regolith strongly influence geomorphic processes across a wide range of scales. In rivers, the supply rate and grain size (D) of sediments coarse enough to move as bedload ($D > 2$ mm), are first-order controls on: channel slope (Howard, 1980; Sklar and Dietrich, 2006), rates of river incision into bedrock (Sklar and Dietrich, 2004; Whipple, 2004), channel planform and cross-sectional geometry (Leopold and Wolman, 1957; Parker et al., 2007), and the quality of aquatic habitat (Kondolf and Wolman, 1993; Meyer and Griffith, 1997). On hillslopes, the size and abundance of rock fragments affect chemical weathering rates (White and Brantley, 2003; Yoo and Mudd, 2008), nutrient supply (Vitousek et al., 2003), hydrologic response (Poesen and Lavee, 1994), and surface erosion rates (Granger et al., 2001). However, little theory or data are available to guide predictions of the size and mass fraction of rock fragments on hillslopes and supplied to channels at the landscape scale (Attal and Lavé, 2006; Sklar et al., 2006).

Hillslopes are the primary source of sediments supplied to and transported by river channels. Rock fragments are produced by processes that convert rock to soil (Heimsath et al., 1997), such as chemical weathering (Yoo et al., 2007) and tree throw (Phillips and Marion, 2004), by physical weathering of bedrock outcrops (Hales and Roering, 2005), and by landslides, both shallow and deep-seated (Casagli et al., 2003). In soil-mantled landscapes, rock fragments in soils are a potential source of bedload material, although weathering in the soil column can reduce the size, abundance, and durability of rock fragments before they reach the channel. Rock fragment abundance measurements are part of standard soil characterization techniques, however, most analysis of soil grain size distributions has focused on particles less than 2 mm (Shirazi and Boersma, 1984; Hwang et al., 2002). An exception has been work focused on saprolite weathering and size reduction of cobbles and boulders within a soil matrix (e.g. Hendricks and Whittig, 1968; Fletcher et al., 2006).

Rock fragment size and abundance should depend on mechanical and chemical properties of the bedrock parent material, climatic factors such as temperature and precipitation,

and geomorphic factors such as erosion rate, hillslope gradient, soil depth, and dominant hillslope transport process. It is reasonable to expect that rock fragments in soils will be larger and more abundant where underlying bedrock is stronger and more resistant to mechanical weathering, in cold or dry environments where chemical weathering is inhibited, and where rapid erosion rates drive steep slopes, thin soils, and brief particle residence times in soils.

Previous investigations of rock fragments in soils have focused primarily on the occurrence of surface accumulations (Poesen and Lavee, 1994) and more generally on vertical movement within the soil column (Phillips et al., 2005). Surface armoring, as documented in many climatic and lithologic settings, is caused by a range of processes including bioturbation, tree throw, freeze–thaw, and surface erosion by wind, overland flow, and tillage (Poesen and Lavee, 1994). Surface cover by rock fragments affects infiltration rates and overland flow velocity (Abrahams and Parsons, 1994; Rieke-Zapp et al., 2007), and can inhibit soil erosion (Granger et al., 2001; Sharmeen and Willgoose, 2007). Rock fragment concentration at the surface has been shown to correlate with bulk rock fragment abundance within the soil column (Simanton et al., 1994), and where rock fragment cover is high vertical profiles show surface coarsening (Poesen et al., 1998; Nyssen et al., 2002). Despite the progress made in understanding the patterns and effects of vertical sorting of rock fragments in soils, much more work is needed before we can reliably predict the landscape-scale variation in the size distribution and abundance of soil rock fragment supplied by hillslopes to channels.

Soils databases are a largely unexploited resource for gaining insight into landscape-scale patterns of rock fragment size and abundance on hillslopes. In the United States, the National Resource Conservation Service (NRCS) maintains a set of databases with pedon-specific records of particle size distributions, which include measurements of rock fragments up to 250 mm in diameter (Burt, 2004). In this paper, we analyze data from the NRCS databases, seeking patterns in rock fragment abundance and size distribution. We focus on elevation gradients where temperature and precipitation vary systematically with elevation, and limit the analysis to hillslope locations where we can reasonably assume size distributions reflect local soil production processes. The key questions we ask are: (1) Do the databases contain useful and reliable measurements of rock fragments in soils on hillslopes? (2) Is there a correlation between the abundance of rock fragments and the characteristic (median) rock fragment grain size? (3) Is there an apparent influence of mean annual precipitation and temperature on rock fragment size distributions? (4) Do rock fragments typically constitute a distinct mode in a bimodal soil particle size distribution or do they occur as the coarse tail of a unimodal distribution? (5) How are rock fragments distributed vertically within the soil column? Our goal is to test the utility of the soils databases and to identify landscape-scale patterns to guide more focused studies on the production of rock fragments and their delivery to river channels.

Study Areas

We focus on three regions in the western United States: the Hawaiian Islands (Islands of Hawaii and Maui), the northern Sierra Nevada Mountains of California and the eastern Cascade Mountains of central Washington (Figure 1). We chose sites in areas where previous researchers have explored the dynamics of landscape evolution in ways relevant to our over-arching question of what controls the size and abundance of rock fragments on hillslopes. Each location is outside the influence
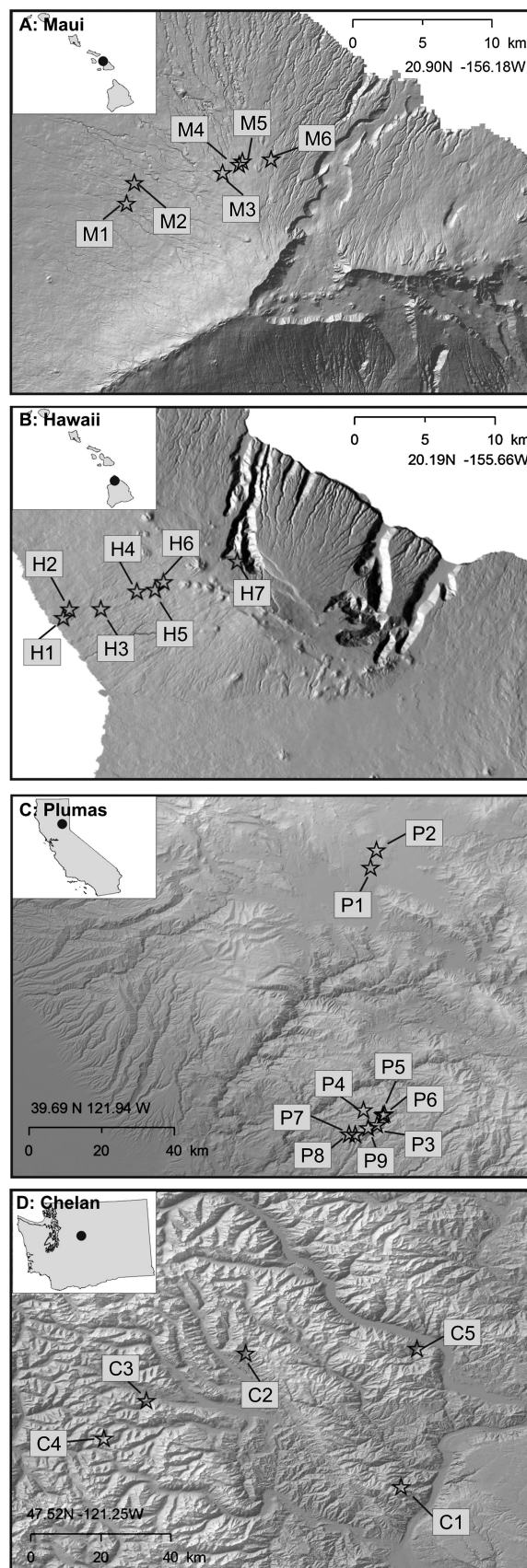
Figure 1. Study site locations. Maps show pedon sample sites in the counties of: (A) Maui, Hawaii, (B) Hawaii, Hawaii, (C) Plumas, California (northern Sierra Nevada Mountains), and (D) Chelan, Washington (eastern Cascade Mountains). Latitude and longitude data refer to zero point on scale bar. Table I provides information on pedon location and site attributes. Maps based on data from the National Elevation Dataset. Digital elevation data available from the US Geological Survey.

of recent volcanism, and all pedons examined are below the elevation of Pleistocene glaciation (Burbank, 1991; Reasoner *et al.*, 2001). For each region, we selected one or two counties because the NRCS data are tabulated by county, and examined every pedon in each county to test the utility of the NRCS data for hillslope rock fragment characterization. Only the fraction of the pedon locations that we deemed suitable for analysis of soil grain size distributions (described in detail later) are mapped in Figure 1.

The Hawaiian Islands provide a unique natural experiment to study the influence of climate on soil development (e.g. Chadwick *et al.*, 2003; Vitousek, 2004), in part because of the uniform underlying basaltic lithology (Wolfe and Morris, 1996). We chose the counties of Hawaii (the 'big island') and Maui (Figures 1A and 1B) because those islands are the youngest of the chain, and because the NRCS pedon data includes previously published measurements from a well-studied set of chronosequences (Crews *et al.*, 1995; Schuur *et al.*, 2001; Chadwick *et al.*, 2003; Vitousek *et al.*, 1997). On both islands, dry and warm conditions at lower elevations contrast with wet and cold conditions at higher elevations. The chronosequence pedons are on the northwest side of the Hawaii Kohala volcano in the Hawi volcanics, and on the northwest side of the Maui Halakealā volcano, in the Kula volcanics (Crews *et al.*, 1995; Schuur *et al.*, 2001; Chadwick *et al.*, 2003; Vitousek *et al.*, 1997). All of the pedon sites are on lava flows dated between 120 ka and 260 ka on Hawaii and 140 ka to 950 ka on Maui (Wolfe and Morris, 1996; Sherrod *et al.*, 2007). Because of the similarity in lithology and environmental conditions, and the overlap in age, between the Hawaii and Maui pedons, we lump these two Hawaiian Island data sets in the quantitative analysis later. However, for clarity we maintain the distinct county names in tabulating and plotting the data.

Plumas County, California, in the northern Sierra Nevada Mountains, is underlain by metamorphic, volcanic, and granitic rocks (Lydon *et al.*, 1960; Burnett and Jennings, 1962). There, deep canyons dissect a low relief surface capped by andesites, andesitic mudflows and volcanic sedimentary rocks (Wakabayashi and Sawyer, 2001). Riebe *et al.* (2000, 2004) explored the dependence of soil weathering on climate and erosion rates in this region. Pedon locations in the NRCS database are underlain primarily by metamorphic and volcanic lithologies, in an area with only minor variation in temperature and precipitation (Figure 1C).

The Pacific Northwest Cascade Range has a well-documented orographic effect, which Reiners *et al.* (2003) used to demonstrate a close coupling between precipitation and long-term erosion rate. We selected Chelan County, Washington, for analysis, where the NRCS pedon locations encompass a precipitation gradient across the windward elevation gradient of the range (Figure 1D), with relatively dry conditions at lower elevations contrasting with wet conditions at higher elevations. The region is underlain primarily by volcanic and metamorphic rocks (Tabor *et al.*, 1987).

Methods

Database selection

We evaluated the four online relational databases maintained by the NRCS for their utility in examining grains size distributions in the soil column. The Soil Survey Laboratory (SSL) database and the associated field site entries stored in the National Soil Information System (NASIS) database are the most appropriate. The SSL and NASIS databases contain site-specific pedon information, compiled from the original fieldwork and laboratory

analysis (Soil Survey Division Staff, 1993). The NRCS subdivides pedon analyses into three types: research, characterization, and geomorphology-stratigraphy projects. We chose characterization pedons for this study because they best represent the grain size distribution in a specific locality. We downloaded all pedon data used in this study from the NRCS National Soil Survey Center Soil Survey Laboratory website (Soil Survey Staff, 2008). The website interface allows users to select data for download from component tables within the SSL and NASIS database system. We used the following three tables: (1) SSL Supplementary Tier 1 (SSL-T1), which contains laboratory sieve data for grains < 75 mm down to 0·002 mm, and soil horizon type and depth; (2) SSL Supplementary Tier 2 (SSL-T2), for field- and laboratory-calculated pedon data for grains > 75 mm; and (3) NASIS data tables, which contain descriptive climatic, topographic, and lithologic information. We also used the Pedon and Site tables in the NASIS database, which provide pedon identifying codes and site location latitude and longitude. Supporting information available online provides a more detailed description of database fields and methods.

Pedon selection

Only a fraction of the pedons listed in the SSL and NASIS databases are useful for characterizing rock fragment abundance and size distributions, and for exploring landscape-scale influences on rock fragment production and supply to river channels. We downloaded data for every available pedon in each of the four study counties, and retained or eliminated pedons based on the following criteria. We excluded records that lack location data, have incomplete horizon information, or where we found irresolvable conflicts between data in the SSL grain size tables and the pedon field descriptions in the NASIS database. To limit our analysis to hillslopes with active soil production, we used the field descriptions and mapped locations to exclude all pedons in valley bottoms, terraces, glacial features and other topographic settings where long-term net accumulation is likely. For the Hawaiian Island data we restricted our analysis to soils located away from vent deposits in the Hawi or Kula volcanic series, and on similar aged flows. Finally, to focus on locations where the mobile soil column extends down to saprolite or bedrock, we excluded data from pedons where the field descriptions and horizon labels do not indicate the depth of bedrock.

Of the 83 pedons examined, we found that 27 (33%) met our data quality and sediment production terrain criteria. The percentage of usable pedons was remarkably similar across regions: 26% in Plumas County and 35% in both Chelan County and the two Hawaiian counties. The reasons for excluding pedons varied by region and likely reflect a combination of regional data needs (i.e. hillslope studies on the Hawaiian Islands versus agricultural characterization in Plumas and Chelan Counties), and errors introduced in consolidating regional or state data into the national database (see supporting information for details). In general, data quality improves with more recent pedon sample collection dates.

Data manipulation

The SSL databases report soil grain size data for individual horizons of variable thickness. Assuming that the entire soil column contains hillslope-derived rock fragments potentially available for supply to channels, we extended our analysis from the base of the surface organic layer (O horizon) down to the top of the saprolite or bedrock. We truncated the soil column at the top of the C-horizon because the NRCS methods define

the C-horizon as little affected by pedogenic processes, consisting of sediment, saprolite, or bedrock (Soil Survey Staff, 2006). If the rate of soil production declines with soil thickness, as has been quantified across diverse landscapes (Heimsath *et al.*, 1997, 1999), bedrock to soil conversion may be negligible where depth to bedrock exceeds a maximum soil production depth (Heimsath *et al.*, 2000; Roering *et al.*, 2002); hence, it is possible that little active conversion of rock to soil is occurring in the thickest pedons.

We reconstructed depth-integrated grain size distributions by averaging the mass fraction of each grain-size class in each horizon, weighted by horizon thickness. We then calculated the rock fragment abundance (F_{RF}) as the fraction of the total soil mass in size classes greater than 2 mm. To focus on the size distribution of rock fragments, we divided the mass fraction of each size class > 2 mm by F_{RF}, to create a normalized cumulative rock fragment size distribution for each pedon. To characterize the central tendency of the rock fragment (> 2 mm) distribution we calculated the median rock fragment size (D_{50RF}) for the soil column. A detailed description of the data manipulation methods is provided in the supporting information.

Data quality control

To assess the quality of the NRCS pedon data for characterizing the size distribution of rock fragments we asked: Are the sample sizes large enough to adequately represent the coarse tail of the grain size distribution? Are the database entries for pedon location and geomorphic setting sufficiently accurate to distinguish between sites of active soil production and sites where net deposition is occurring? We reviewed the NRCS collection and analysis methods (Burt, 2004; USDA NRCS, 2005), spoke with researchers and database managers at the National Soil Survey Laboratory, and observed NRCS staff field pedon characterization. As described later, we are confident in the quality of the data for this exploratory study of the rock fragment grain size distribution in soil-mantled hillslopes.

Minimum sample volume

In field sampling for rock fragments, large sample volumes are required to limit measurement uncertainty to acceptable levels. Smaller samples are sufficient when only the sand and finer particle sizes are of interest; this provides a partial explanation for the paucity of published data on rock fragment abundance in soils. For our purposes, a sufficiently large sample volume is important for two reasons: (1) the presence or absence of a single large rock can have a strong influence on the estimate of the mass fraction of rock fragments in the sample; and (2) rock fragments constitute a coarse tail of the bulk soil particle size distribution and the tails of a distribution are inherently more difficult to characterize than the central tendency.

Numerous methods are used to define the minimum sample mass for sampling particle size distributions in river beds (Bunte and Abt, 2001). Here we adapt two conventional methods to test if the pedon sample sizes provide sufficiently precise estimates of rock fragment abundance and size distribution. De Vries (1970) showed that the percent error in estimating the total mass of the sample is proportional to the fraction of the total mass contributed by the largest particle. Church *et al.* (1987) empirically determined that the uncertainty in the estimate of the mass fraction of each size class, represented by the coefficient of variation, will not exceed 10% if the largest particle contributes no more than 0·1% of the total sample mass.

Because the soils databases do not provide information on the total sample mass, we must convert from mass to volume to assess the sample size. NRCS sampling protocol

(Burt, 2004) specifies that a soil pit from which the sample is taken should cover a minimum area at the surface of 1 m². We estimate the total sample volume as the product of the pit area and the total depth to the bottom of the sample. The databases also do not report the variation in particle density with grain size, we therefore assume a uniform particle density and sample porosity to estimate the total sample volume.

The minimum required sample volume (V_{min}) can therefore be expressed as a function of the maximum grain size considered (D_{max})

$$V_{min} = \frac{\pi D_{max}^3}{6(1 - n)f_D} \tag{1}$$

where n is sample porosity and f_D is the fraction of the total sample volume represented by the largest particle, which is assumed to be nominally-spherical. The minimum sample volumes required with $f_D = 0.001$ (0·1%) are practical to obtain for size distributions with D_{max} in the coarse sand or fine gravel size classes, but become impractical for $D_{max} > 32$ mm. Church *et al.* (1987) recommend less stringent criteria for coarser gravel and cobble-sized largest grains, such that $f_D = 0.01$ for 32 mm < $D_{max} < 128$ mm and $f_D = 0.05$ for $D_{max} > 128$ mm.

Figure 2 shows the estimated sample volume for each pedon compared to the minimum sample volume calculated using Equation 1 (for $f_D = 0.001$, 0·01 and 0·05), with D_{max} set by the largest particle reported for each pedon; for this calculation we assume $n = 0.3$. The stepped variation in V_{min} with increasing D_{max} recommended by Church *et al.* (1987) is shown by the heavy line. As shown in Figure 2, all of the estimated pedon sample volumes exceed the recommended V_{min}. Sixteen (57%) of the pedons have $D_{max} = 400$ mm and 50% of these pedons not only meet the criterion for grains > 128 mm, but also exceed $f_D = 0.01$. Of the remaining 10 pedons, all exceed the most stringent criterion of $f_D = 0.001$. We conclude that the sample sizes are sufficiently large to reliably characterize the rock fragment size distributions within each pedon.

Pedon site information

As an independent check on the pedon site information in the NASIS database we used the latitude and longitude information and the narrative location descriptions to locate the pedon sites
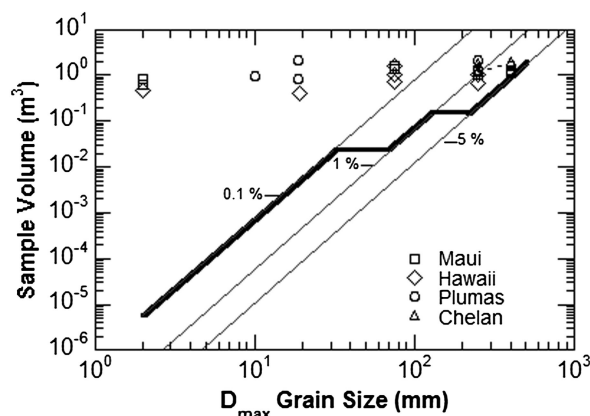
Figure 2. Minimum sample volume as a function of maximum grain size (D_{max}). Thin lines indicate volume needed (Equation 1) so that the mass fraction of the largest grain (f_D) does not exceed the labeled percentage. Thick solid lines indicate the stepped criteria recommended by Church *et al.* (1987) for minimum sample volume for three size classes: $f_D = 0.1\%$, 1% and 5% for $D_{max} < 32$ mm, 32 mm $< D_{max} < 128$ mm, and $D_{max} > 128$ mm respectively. Symbols show estimated sample volumes as a function of D_{max} for each pedon (modified from Bunte and Abt, 2001).

on US Geological Survey (USGS) topographic maps and Google Earth satellite and terrain imagery. We then evaluated the NASIS database narrative descriptions of the site geomorphology and slope position, and mapped topography to verify that pedon sites were not located in depositional units. For each of the pedons included in the analysis later, we found no inconsistencies in location or apparent topographic position between the database information and site location attributes evident on the topographic maps and Google Earth images.

Although the qualitative slope position descriptions in the NASIS database are reliable for excluding depositional settings such as terraces and fans, we judged the quantitative measures of hillslope gradient to be unreliable for testing for the influence of slope on rock fragment abundance and size distribution, because slope values for the NRCS pedon descriptions are collected by hand level or clinometer over an indeterminate length (USDA NRCS, 2007). The NASIS database also includes fields for curvature (upslope and cross-slope), but very few records have entries in this field.

Bedrock lithology is well-constrained for the Hawaiian Island sites, however, the NASIS parent material data for the Plumas and Chelan sites are often vague or entirely absent. To better constrain the site lithology we located the pedon sites on regional geology maps (Lydon *et al.*, 1960; Burnett and Jennings, 1962; Tabor *et al.*, 1987; Ludington *et al.*, 2007) and used data from the NRCS Official Series Descriptions (USDA NRCS, 2011). In many cases, NRCS data (from both NASIS and soil series descriptions) indicate parent materials different from mapped bedrock types.

Results

Here we present analysis of the grain size distributions of the 27 pedons that satisfied our criteria for data quality and relevance for understanding the controls on size and abundance of rock fragments on soil-mantled hillslopes (Table I). We first present the grain size distribution curves, and then report co-variation between rock fragment abundance (F_{RF}) and median fragment size (D_{50RF}), and variation in F_{RF} and D_{50RF} with elevation, mean annual precipitation, and temperature. We then analyze the occurrence of bimodal distributions and variation in rock fragment abundance within pedon depth profiles. To quantify apparent patterns in the data, we tested linear, power and exponential relations using least-squares regression, and include in the data plots the functions which best fit the data, but only where the regression significance exceeds the 90% confidence level ($p < 0.1$).

Grain size distributions

Figure 3 shows the cumulative grain size distributions for each of the 27 pedons, grouped by county. We plotted the cumulative distributions for the entire soil sample ($0.002\,\text{mm} < D$ 400 mm) in the left panels (Figures 3A, 3C, 3E, and 3G), and for the rock fragment fraction only ($2\,\text{mm} < D < 400\,\text{mm}$) in the right panels (Figures 3B, 3D, 3F, and 3H). Within each region, the pedons are numbered in order of increasing mean annual precipitation. Bimodal distributions (as described later) are indicated by solid lines and unimodal distributions by dashed lines.

We find rock fragments in the soils of all three regions, with rock fragments in all the Plumas and Chelan samples, and in nine of the 13 Hawaiian Island samples. Where rock fragments occur, F_{RF} ranges from 3% in Hawaiian site M3 to 80% in Chelan site C2. The Hawaiian Island pedons lacking rock

fragments are at wetter, higher elevations on each island. The range of D_{50RF} is narrowest in the Hawaiian Island samples, where the D_{50RF} ranges from 4 mm to 33 mm, while in both the Plumas and Chelan samples, the D_{50RF} ranges from 4 mm to 167 mm.

Co-variation of D_{50RF} and F_{RF}

We do not expect rock fragment abundance (F_{RF}) and median grain size (D_{50RF}), our two principal metrics of interest, to be independent. Soils with more rock fragments are likely to also have coarser rock fragments. Here we find a strong positive correlation between D_{50RF} and F_{RF} within each region, as shown in Figure 4. The variation in D_{50RF} with F_{RF} is well-fit by power expressions (Table II), with the Plumas and Chelan sites showing a greater sensitivity (larger exponent) than the Hawaiian Island sites. We have excluded Plumas site P8 (Cook's $D = 8 > 1$, strongly indicates an outlier, $p < 0.0001$; Cook and Weisber, 1982); the anomalous behavior of P8 may be because this is the only pedon with a granitic lithology.

Correlations with elevation and climate

Rock fragment abundance and median grain size vary with elevation for all regions (Figure 5). Elevation can be considered a proxy for the combined influences of precipitation and temperature, although other factors such as erosion rate and lithology may also vary with elevation. For the Hawaiian Island samples, rock fragments become significantly more abundant and coarse as elevation decreases, while the opposite trends occur in the Chelan samples (the Plumas trends are not significant). The patterns are more consistent for F_{RF} than D_{50RF}, as indicated by the scatter around the exponential functions fit to illustrate the trends (Figures 5A and 5B; Table II).

One possible explanation for the differing trends is the variation in precipitation and temperature with elevation. In the Hawaiian Islands, the pedon sites are located on the leeward side of the topographic crest, while the Chelan and Plumas sites are on the windward side of the topographic divide (Figure 1; Table I). Although the rate of decrease in temperature with elevation is similar for all sites, there is a gradient in latitude between sites, from the warmer Hawaiian Islands to the colder, higher latitude Chelan and Plumas sites.

In Figure 6, we explore the potential influence of climate on rock fragment abundance, by plotting the variation in F_{RF} with mean annual precipitation (P_{ma}) and mean annual temperature (T_{ma}). The only significant trends are in the Hawaii data, where F_{RF} decreases with increasing precipitation (Figure 6A) and the corresponding decrease in temperature (Figure 6B) with higher elevation. For comparison with the uniform lithology Hawaiian Island data, we also plot the mixed-lithology Chelan and Plumas data. We have fit exponential relations to the Hawaii Island data ($p < 0.005$) in Figure 6, although we have no theory to suggest this is the most appropriate functional relationship between F_{RF} and P_{ma} and T_{ma}. Because D_{50RF} is highly correlated with F_{RF} (Figure 4), the pattern of variation in D_{50RF} with P_{ma} and T_{ma} is similar to F_{RF}, although with greater scatter.

Bimodal versus unimodal distributions

Are rock fragments in soils typically the coarse tail of a unimodal grain size distribution, or the coarse mode of a bimodal soil size distribution? Answering this question is essential for modeling coarse sediment supply to rivers (e.g. Sklar *et al.*, 2006). In Figures 7a and 7b we plot two sets of hypothetical

Table I. Pedon summary information.

Site	NRCS-ID	Latitude	Longitude	Elevation (m)	Precipitation (mm)	Temperature (°C)	Lithology	F_{RF} (%)	D_{50RF} (mm)	Modal	Breakpoint (mm)	Soil depth (m)	NRCS soil Series name
Maui County, Hawaii													
M1	84P0044	N20°47'40"	W156°20'00"	715	560	20[a]	basalt	6	5	uni-	2·0	1·60	Keahua/Kamaole
M2	83P0881	N20°47'40"	W156°19'40"	870	650	19	basalt	29	21	bi-	4·8	1·10	Pane
M3	98P0264	N20°48'00"	W156°16'00"	1269	1450	16[a]	basalt	0	-	uni-	2·0	1·40	Olinda
M4	97P0246	N20°46'52"	W156°15'18"	1378	2200	16[a]	basalt	3	4	uni-	2·0	1·00	Honomanu
M5	97P0247	N20°48'27"	W156°15'11"	1378	2435	16[a]	basalt	0	-	uni-	4·8	0·80	Honomanu
M6	97P0248	N20°58'30"	W156°15'00"	1378	2759	16[a]	basalt	0	-	uni-	2·0	0·60	Amalu
Hawaii County, Hawaii													
H1	92P0626	N20°04'47"	W155°51'17"	77	160[c]	23	basalt	47	31	bi-	2·0	1·00	Holikau[h]
H2	92P0623	N20°05'08"	W155°55'02"	185	180[c]	23	basalt	62	28	bi-	2·0	0·65	Holikau[h]
H3	92P0625	N20°05'10"	W155°49'45"	356	270[c]	23	basalt	57	33	bi-	3·1	0·70	Puu Pa
H4	92P0628	N20°05'53"	W155°48'18"	674	570[c]	20	basalt	33	27	bi-	3·1	1·03	Puu Pa
H5	92P0627	N20°05'58"	W155°47'34"	792	762	20[b]	basalt	18	23	bi-	3·1	1·62	Waimea
H6	92P0622	N20°06'17"	W155°47'13"	992	930[c]	19	basalt	9	9	bi-	4·8	0·41	Waimea
H7	93P0419	N20°79'13"	W155°44'14"	1254	3000[c]	17	basalt	0	0	uni-	4·8	0·45	Waimea
Plumas County, California													
P1	84P0755	N40°20'09"	W121°05'45"	1586	894[a]	10[a]	basalt[d]	45	53	bi-	19	1·17	Tahand
P2	84P0756	N40°22'43"	W121°04'53"	1788	996	9	basalt[d]	58	21	bi-	36	1·12	Swainow
P3	98P0289	N39°41'55"	W121°04'47"	1548	1955	10	basalt[e]	68	96	bi-	44	1·26	Timberisland
P4	98P0290	N39°44'06"	W121°06'48"	1570	1956	10	meta-volca[e]	29	7	bi-	36	2·13	Stagpoint
P5	98P0287	N39°43'23"	W121°03'56"	1623	1956	9	meta-volcanic[d]	57	132	bi-	44	1·61	Stagpoint
P6	98P0286	N39°43'29"	W121°03'41"	1654	1956	9	meta-volcanic[e]	38	9	bi-	44	2·06	Dejonah
P7	97P0310	N39°40'30"	W121°08'58"	1396	1965	11	basalt, breccia[f]	37	4	uni-	25	2·16	Shakeridge[i]
P8	97P0311	N39°40'27"	W121°08'00"	1273	2032	11	quartz diorite[f]	6	3	uni-	10	0·97	Bonneyridge[i]
P9	97P0309	N39°41'24"	W121°06'25"	1463	2032	10	basalt[e]	24	4	uni-	25	0·86	Powderhouse[i]
Chelan County, Washington													
C1	87P0751	N47°37'28"	W120°19'20"	840	50	6	gneiss[g]	40	13	bi-	16	1·28	Ardenmont[i]
C2	87P0755	N48°58'04"	W120°43'21"	1070	125	4	gneiss[g], tuff	75	167	bi-	19	1·23	Wedge[i]
C3	87P0753	N47°50'46"	W120°58'40"	720	193	5	gneiss[g], tuff	19	8	bi-	44	0·78	Line[i]
C4	87P0752	N47°44'54"	W120°05'13"	1220	200	4	migmatite[g]	66	44	bi-	19	1·94	Chickman[h]
C5	96P0394	N47°58'49"	W120°16'49"	512	356	8	gneiss[g], tuff, mixed[f]	25	4	uni-	25	1·32	Mansonia

Note: Precipitation = mean annual precipitation, source: NASIS database; Temperature = mean annual temperature, source: NASIS database; Lithology = bedrock lithology, source: NASIS database; RF = rock fragment abundance, mass % of total sample; F_{RF} = mass fraction of RF; D_{50RF} = median grain diameter of RFs; Breakpoint = median value (log-transformed) between the coarse and fine modes of the bimodal distributions, and the largest grain size of the unimodal distributions; NRCS Soil Series Name, Soil Name as Correlated NASIS database.

[a] PRISM Climate Group (2008).

[b] Calculated environmental lapse rate based on local NASIS mean annual temperature data.

[c] Chadwick *et al.* (2003).

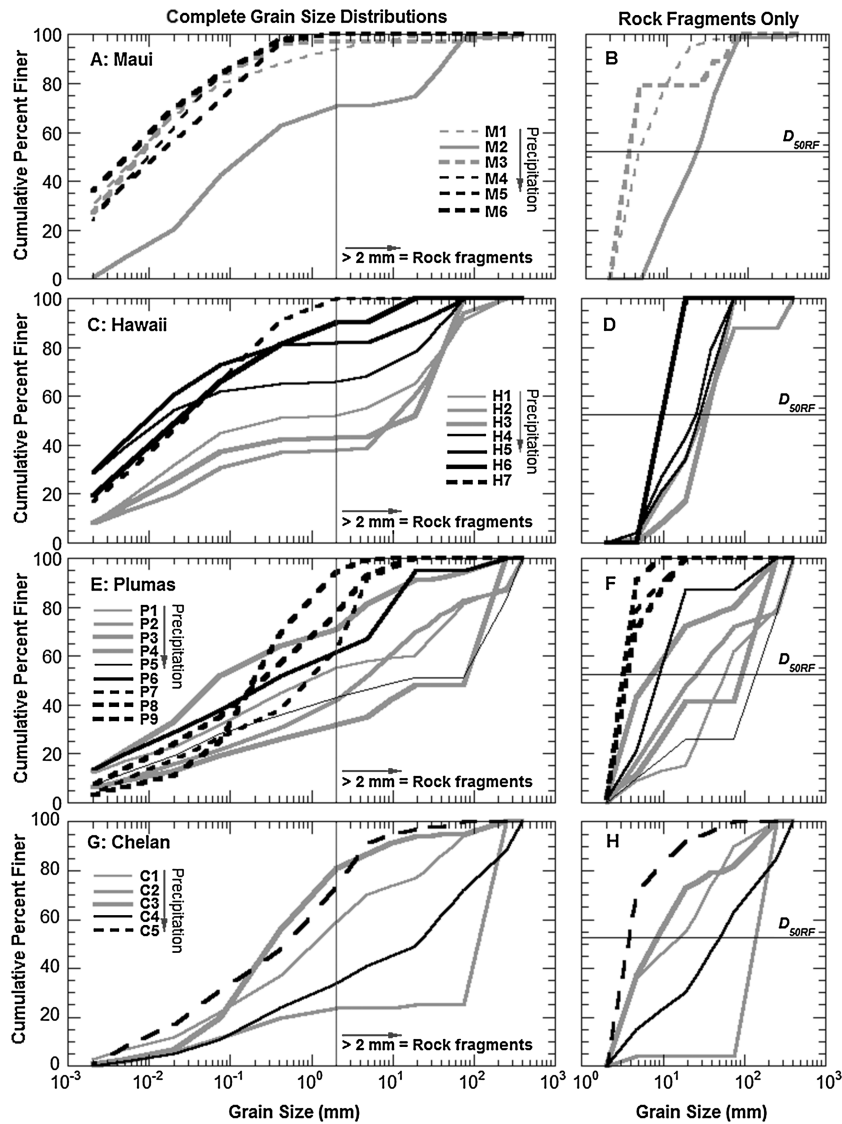[d] Lydon *et al.* (1960).

[e] Burnett and Jennings (1962).

[f] USDA NRCS (2011).

[g] Tabor *et al.* (1987).

[h] Series name not found in online database.

[i] Soil series type locality.

Figure 3. Cumulative grain size distributions for pedons from each region. Left panels (A, C, E, G) show depth-averaged distributions for all size fractions, right panels (B, D, F, H) show size distributions of rock fragments only ($D > 2$ mm), normalized by the rock fragment mass fraction (F_{RF}). Pedon sites are listed in order of increasing mean annual precipitation. Dashed lines indicate unimodal distributions, solid lines indicate bimodal distributions.
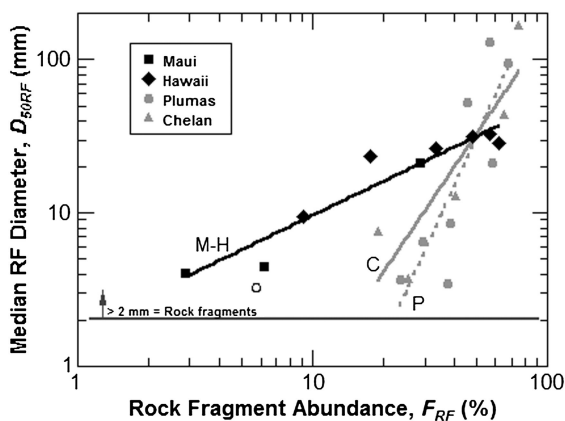
Figure 4. Variation in median rock fragment grain size (D_{50RF}) with rock fragment mass fraction (F_{RF}). Lines indicate best-fit power functions; $p < 0.0001$ (Maui-Hawaii), $p = 0.0090$ (Plumas) and $p = 0.039$ (Chelan). Maui and Hawaii data combined in this and all subsequent regressions. Open circle indicates outlier (site P8) excluded from this and all subsequent fits to the Plumas data; see text for exclusion criteria.

bulk soil grain size distributions as reference cases to evaluate the occurrence and patterns of bimodality in measured grain size distributions. In each hypothetical case F_{RF} varies between 2% and 50%. In the first case (unimodal), variations in F_{RF} and D_{50RF} occur due to shifts in the mean and standard deviation of a single log-normal distribution (Figure 7a). In the second case (bimodal), the rock fragment and finer soil particle distributions are distinct log-normal curves and F_{RF} varies directly with the relative contribution of the mass fraction of the coarse distribution to the total soil mass (Figure 7b).

Figure 7 also shows the pedon bulk grain size distributions as probability density functions by mass, for each of the four regions. As in Figure 3, dashed lines indicate unimodal distributions. Visual inspection of cumulative (Figure 3) and probability (Figures , 7c–7f) distribution plots allowed us to categorize the distributions as unimodal or bimodal, with bimodal distributions containing pronounced plateaux in the cumulative curves, and low points or gaps in the probability curves. Our approach is similar to methods used to detect bimodality in studies of river bedload transport (Wilcock, 1993; Smith *et al.*, 1997) and sediment provenance (Sun *et al.*, 2002; Radoane *et al.*, 2008). We inspected the original

Table II. Regression statistics.

Figure	Data set	Best-fit equation[a]	n	R^2	p
4	Maui-Hawaii	$D_{50RF} = 1.8\ F_{RF}^{\ 0.74(\pm0.09)}$	9	0.91	<0.0001
4	Plumas	$D_{50RF} = 0.00005\ F_{RF}^{\ 3.4(\pm0.89)}$	8	0.71	0.0090
4	Chelan	$D_{50RF} = 0.005\ F_{RF}^{\ 2.3(\pm0.65)}$	5	0.80	0.039
5A	Maui-Hawaii	$F_{RF} = 89\ e^{-0.002(\pm0.0005)\ Z}$	9	0.73	0.0036
5A	Chelan	$F_{RF} = 8\ e^{0.0018(\pm0.0006)}$	5	0.74	0.0062
5B	Maui-Hawaii	$D_{50RF} = 43\ e^{-0.0015(\pm0.0001)\ Z}$	9	0.53	0.026
5B	Chelan	$D_{50RF} = 0.33\ e^{0.004(\pm0.0016)\ Z}$	5	0.75	0.058
6A	Maui-Hawaii	$F_{RF} = 55\ e^{-0.0015(\pm0.0004)\ P}$	9	0.71	0.0042
6B	Maui-Hawaii	$F_{RF} = 0.006\ e^{0.39(\pm0.09)\ T}$	9	0.74	0.0031
8	All	$D_{bp} = 92\ e^{-0.17(\pm0.02)\ T}$	27	0.73	<0.0001

[a]D_{50RF} = median rock fragment grain size, F_{RF} = mass fraction of rock fragments, Z = elevation (in meters), P = precipitation (in millimeters, T = temperature (°C).
[b]Standard error of regression slope in parentheses.

horizon data to avoid designating a distribution as bimodal because of a single large rock fragment; we also confirmed our mode determination using Gradistat (Blott and Pye, 2001), a grain-size distribution plotting software that outputs the number of modes in a distribution.

As shown in Figure 7, both distribution types are found in every region, with bimodal distributions occurring in 64% (17 of 27) of the pedons analyzed. Within each region, the unimodal distributions are generally from the finer-grained bulk distributions. Maui has the finest bulk distributions as well as the greatest percentage of unimodal distributions (five of six); in contrast, the Chelan bulk distributions are the coarsest of three regions overall, with only one unimodal distribution. In most cases, bimodal distributions have larger D_{50RF} compared to the unimodal distributions within each regional dataset. For example, all of the Plumas unimodal D_{50RF} values are less than 4 mm while the bimodal D_{50RF} values range from 6 mm to 132 mm. None of the unimodal distributions contains coarse fragments greater than 20 mm; $F_{RF} < 5\%$ for unimodal distributions in all regions.

The pattern of unimodal and bimodal size distributions is most consistent with the second hypothetical case illustrated in Figure 7b, where significant rock fragment abundance and coarseness occurs in a distinct coarse mode. In all regions, the finer modes of the bimodal distributions span the same grain size range as the unimodal distributions. For example, in the Maui samples (Figure 7c) all of the unimodal distributions span a range from 0.001 mm to a maximum of 4 mm, the same range as the fine mode of the bimodal M2 distribution. Unlike the hypothetical unimodal distributions (Figure 7a), we find no unimodal distributions that extend into the size range of the coarse mode of the bimodal distributions; this is well-illustrated in the Plumas and Chelan data (Figures 7e and 7f).

Mean-annual precipitation (P_{ma}) correlates with whether distributions are unimodal or bimodal. Nearly every unimodal pedon (nine of 10) has greater P_{ma} than all bimodal pedons in the same region. Precipitation is even a significant predictor of distribution type when all three regions are lumped together, despite the differences in lithology and other factors. A logistic regression, which describes the probability of obtaining a bimodal soil grain size distribution as a function of P_{ma}, is significant at the 98% confidence level, when all three regions are combined.

'Breakpoints' between modes

An important metric for describing the grain size distributions plotted in Figure 7 is the characteristic grain size associated with the gap, or break, between the coarse and fine modes of
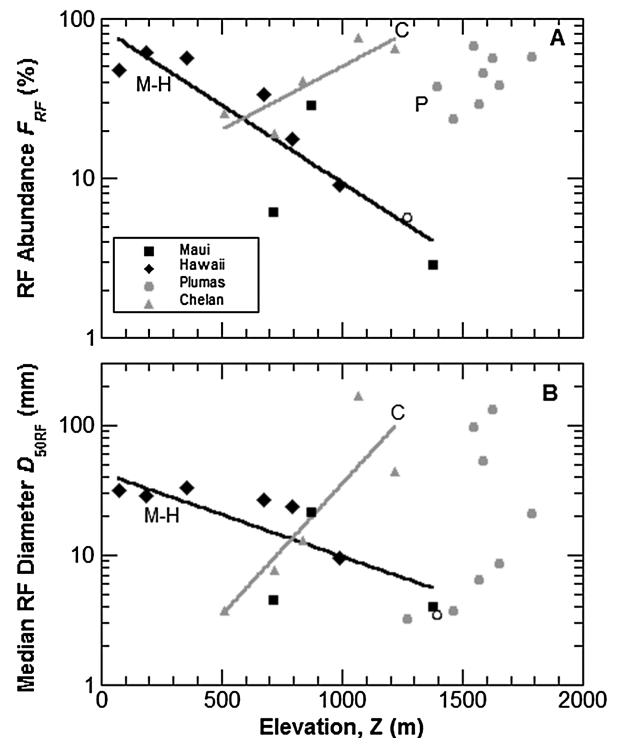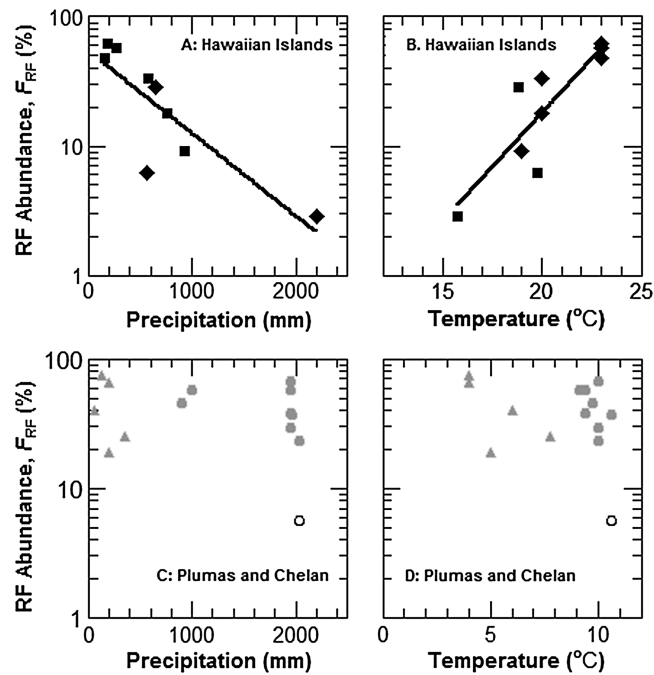

Figure 5. Variation in rock fragment abundance (A) and median rock fragment size (B) with elevation of pedon sample site. Lines indicate best-fit exponential functions; $p = 0.0036$ (Maui-Hawaii) and $p = 0.0062$ (Chelan).

the bimodal distributions, which we term the 'breakpoint' of the distribution. We estimated the breakpoint between modes as the midpoint between the finest grain size bin in the coarse mode and the coarsest grain size bin in the fine mode; we calculated the midpoint as the mean of the log-transformed ('phi') values for the grain-size-bin midpoints. In each case, these limiting grain size bins were apparent visually, and contained less than 3% (typically < 1%) of the mass in the cumulative distribution. We also apply the term 'breakpoint' to the tip of the coarse tail of the unimodal distributions, as a metric of the upper limit of the fine mode when a coarse mode is absent, using the same criteria as earlier for determining the coarsest grain size bin.

Each regional dataset has a consistent and narrow range of breakpoint sizes, indicated in Figures , 7c–7f as a shaded vertical band. For example, in both Maui and Hawaii, the unimodal maximum grain sizes are all between 2 and 4.8 mm, and in the bimodal distributions, the finer-mode maximum grain

Figure 6. Variation in rock fragment abundance with mean annual precipitation and temperature, for (A and B) Hawaiian Island sites, and (C and D) Chelan county sites. Lines indicate best-fit exponential functions; $p = 0.0042$ and $p = 0.0031$ for Maui-Hawaii precipitation and temperature respectively.

size is 2 mm in five of seven pedons, while the coarse mode range begins at either 2 or 4.8 mm (Figures 7c and 7d).

The breakpoint grain size separating fine and coarse modes is larger for the Plumas and Chelan distributions than for the Hawaiian Island distributions. Mean annual temperature is also dramatically different between these two sets of pedon locations. In Figure 8, we plot the breakpoint size against temperature, with unimodal and bimodal distributions distinguished by symbol shading. The variation in breakpoint size with temperature is well-fit by an inverse exponential relationship ($p < 0.0001$); in Figure 8, we fit a single line to the combined unimodal and bimodal data, however, separate regression lines for two distribution types show similar trends. Breakpoint size does not correlate with mean annual precipitation.

Correlations with soil depth

Our analysis so far has focused on the depth-averaged grain size distributions, where the contribution of each soil horizon is weighted by horizon thickness. We next analyze the variation in rock fragment abundance between horizons, as a function of depth below the surface. Figure 9 shows the rock fragment abundance in each soil horizon (f_{RF}) plotted against the depth below the surface to the bottom of the each horizon, for each study region (Figure 9A, 9C, 9E, and 9G). To facilitate comparison between pedons, we plot in the right set of panels the same data normalized to show the cumulative fraction of the total rock fragment abundance for each pedon as a function of the cumulative depth below the surface (Figure 9B, 9D, 9F, and 9H). The dotted line in the normalized plots indicates the 1:1 slope for uniformly distributed rock fragments with depth. Data plotting above or below the line reflect greater rock fragment abundance in the upper or lower portions of the pedon respectively, which we refer to as 'surface-enriched' or 'depth enriched'.

Overall, we do not find any significant trends between bulk F_{RF} and depth-to-bedrock, nor any strong trends in horizon-specific rock fragment abundance (f_{RF}) with depth. Rock fragments occur throughout the range of horizons and in many
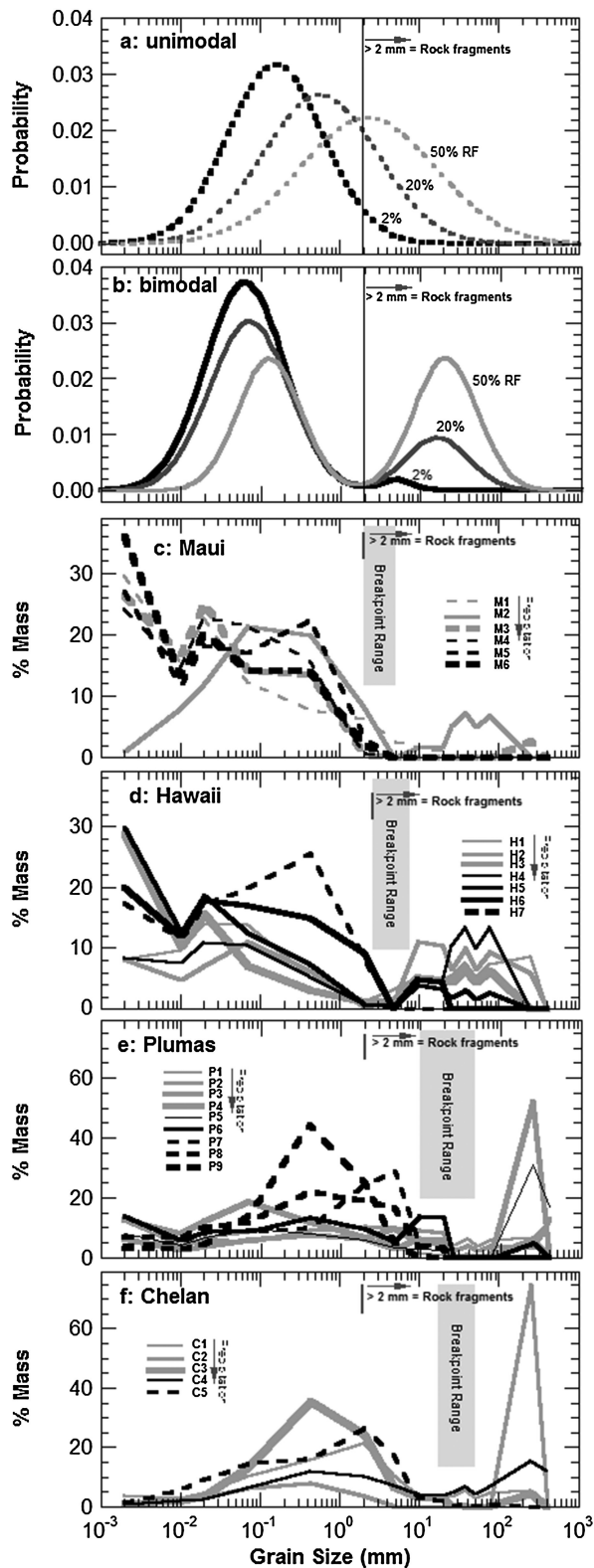
pedons are distributed somewhat uniformly through the soil column (with the exception of the three Maui sites, which also have relatively low F_{RF}). The Hawaii sites show the clearest pattern, with a consistent shift from surface-rich to depth-rich rock fragment depth profiles as precipitation increases (Figure 9D), and bulk F_{RF} decreases (Figure 9C). The Plumas and Chelan sites are dominantly surface-rich, but do not show any trend with precipitation. Overall, 70% (16 of 23) of the pedons have greater than half of the rock fragments in the upper half of the soil column.

Discussion

Soil database utility

The NRCS databases are a useful resource for examining rock fragments in soils. The databases provide sufficient information to identify the pedon sample pits dug on hillslope locations where soils reflect local soil production processes rather than depositional processes. For pedons used by the NRCS to characterize regional soil patterns, the sampling and grain size analysis methods are sufficiently thorough and standardized to trust the quality of the data on rock fragment size and abundance. For the four counties we selected, rock fragments occur in nearly all the pedons that satisfied our data quality criteria (23 of 27), suggesting that the NRCS databases contain a wealth of useful data on rock fragments in soils across a wide range of landscapes.

A major limitation in using the NRCS database to understand controls on rock fragment production in soils is constraining the rock fragment parent material. Rock type was difficult to determine in many of the Plumas and Chelan pedons from the information in the database alone, and we found conflicts between mapped bedrock geology and the lithology of rock fragments reported in the database and soil series descriptions. Soil rock fragment parent material can differ from the bedrock lithology at the base of a pedon, for example where rock fragments are supplied by upslope bedrock outcrops (Poesen et al., 1998) or in layered rock types such as alternating

sandstone and shale, where sandstone rock fragments may overly shale bedrock (Phillips *et al.*, 2005). Because pedon sites chosen for soils characterization are intended to represent a spatially extensive soil series, pedon transects where parent material can be held constant may be difficult to find in the NRCS database, except in regions of unusually uniform lithology such as Hawaii. Even where mapped bedrock geology is uniform, for example in granitic batholiths, subtle variation in mineralogy can have a large influence on rock weathering patterns and rock fragment formation (e.g.Wahrhaftig, 1965; Isherwood and Street, 1976; Dahlgren *et al.*, 1997).
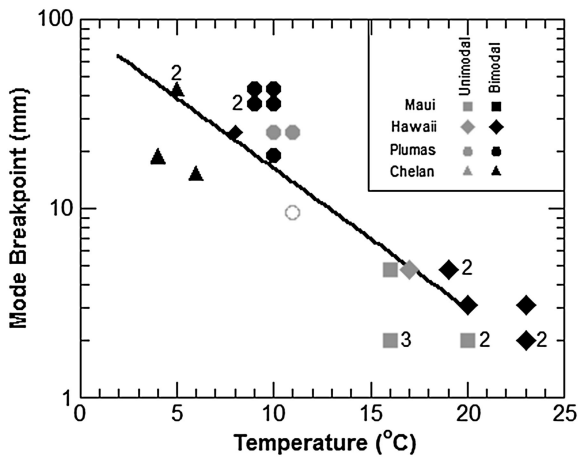
Landscape-scale patterns

Despite the uncertainty introduced by variable lithology, three strong patterns emerge from the data. First, we find a consistent positive correlation between rock fragment abundance (F_{RF}) and median rock fragment size (D_{50RF}). To our knowledge, this is the first time this relationship has been quantified. Power equations fit each regional dataset well, however, the trend of the Hawaiian Island data is distinctly different from the Plumas and Chelan data (Figure 4). This suggests that the scaling between F_{RF} and D_{50RF} may be a useful metric for testing hypotheses for the controls on rock fragment production and weathering (Poesen *et al.*, 1998; Phillips *et al.*, 2005).

Second, we find that bimodal soil grain size distributions are common (Figure 7), occurring in the majority of the pedons we analyzed (17 of 27). Importantly, we find that rock fragments occur primarily in the coarse mode of bimodal distributions, rather than in the coarse tail of unimodal distributions. Explaining the occurrence of bimodal distributions, and the location of the breakpoint between modes near the transition from gravel to sand size classes (Figure 9), provides a challenge for modeling rock fragment production processes (Fletcher *et al.*, 2006) and rock fragment weathering in the soil column (Yoo and Mudd, 2008).

Third, mean annual precipitation correlates with most of the significant patterns of variation in rock fragment size and abundance in this data set. In the Hawaiian sites, where lithology is uniform, F_{RF} declines with increasing precipitation, and the four pedons that lack rock fragments entirely have the highest precipitation rates among the sites. High precipitation rates are also associated with lack of bimodal size distributions; the pedons with unimodal distributions have the highest-ranking precipitation rates in each region (Table I). Precipitation also appears to influence the vertical distribution of rock fragments, with a lack of surface-enrichment correlating with higher precipitation rates, particularly in Hawaii. These results are consistent with field studies showing high surface abundance of rock fragments in arid and semi-arid regions (Simanton *et al.*, 1994; Nyssen *et al.*, 2002).

One possible explanation for the different scaling between F_{RF} and D_{50RF} in the Hawaiian Island versus Plumas and Chelan datasets (Figure 4) is the potential role of rock properties, such as crystal grain size, in limiting the range of rock fragment sizes produced (e.g. Chadwick *et al.*, 2003). The basalt rock fragments in Hawaii and Maui show only a small variation in size, despite a wide variation in rock fragment abundance. In contrast, the Plumas and Chelan rock fragments span a much larger size range, and are derived from multiple lithologies. The anomalous behavior of the only granitic pedon (P8) may reflect the pattern of mineral disaggregation common in granitic rocks (Wahrhaftig, 1965; Graham and O'Geen, 2010) or the distribution of spacing between fractures (Perfect, 1997; Graham *et al.*, 2010)

Figure 7. Idealized and measured grain size frequency distributions, by mass, showing occurrence of unimodal and bimodal distributions. (a) Hypothetical log-normal size distributions illustrating how variation in rock fragment abundance may arise from shifts in the size range of the coarse tail of a unimodal distribution. (b) Hypothetical bimodal distributions composed of two log-normal modes, illustrating how variations in rock fragment abundance could reflect the relative mass fraction of a distinct coarse-grained mode. (c) Maui; (d) Hawaii; (e) Plumas; (f) Chelan sites. Pedon sites are listed in order of increasing mean annual precipitation. Dashed lines indicate unimodal distributions, solid lines indicate bimodal distributions. Grey vertical bands indicate range of 'breakpoint' grain sizes for each region, as defined in the text.

Figure 8. Variation in 'breakpoint' grain size with mean annual temperature. Breakpoint defined as maximum grain size for unimodal distributions and, for bimodal distributions as the mean of the log-transformed maximum fine mode size and minimum coarse mode size. Exponential function fit to highlight trend, $p < 0.0001$. Number of overlapping points indicated.

There is a risk that the trend in breakpoint size with temperature (Figure 8) could be an artifact of differences in rock properties (or other climatic factors) between the uniform basalt of the Hawaiian sites and variable lithology of the Plumas and Chelan sites. We note, however, that basalt is also the parent lithology in several of the Plumas sites, and more importantly that temperature is a first order control on rock weathering rate, as documented and modeled by many authors (e.g. Riebe *et al.*, 2004; West *et al.*, 2005), who have found an inverse exponential Arhenius relation similar in form to our empirical fit to the breakpoint versus temperature data.

We are confident that the finding of bimodal bulk grain size distributions is robust, and not an artifact of soil sampling methods. Although NRCS sampling methods differ for grains larger and smaller than 75 mm, identical laboratory dry sieving methods are used across the full range of observed breakpoints (2 mm to 44 mm) (Burt, 2004; USDA NRCS, 2005; Soil Survey Staff, 2008). Moreover, if the observed bimodal distributions were an artifact of a shift in grain size analysis methods at a specific size (75 mm), we would expect the breakpoint to occur at or near that grain size in all samples; instead we observe a wide range of breakpoint sizes (Figure 8, Table I). Bimodal distributions typically reflect mixing of two distinct populations, and it is possible that distinct coarse rock
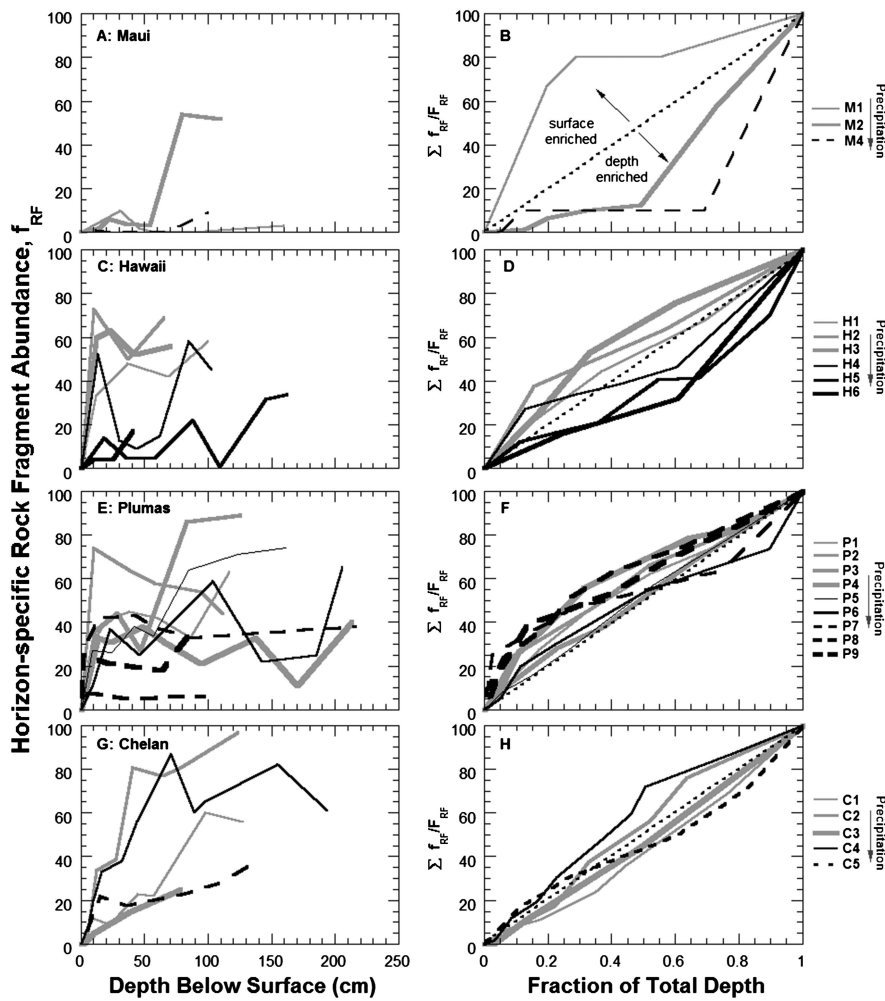
Figure 9. Variation in rock fragment abundance in each soil horizon with depth below surface. Left panels (A, C, E, G) show rock fragment mass fraction in each horizon (f_{RF}) plotted against maximum depth of horizon below surface. Right panels (B, D, F, H) show cumulative fraction of total pedon rock fragments with increasing depth (vertical axis) plotted against cumulative depth below the surface (horizontal axis), normalized by total pedon depth-to-bedrock. Diagonal dotted lines on right panels indicate 1:1 slope for perfectly uniform vertical distribution of rock fragments; curves plotting above this line are 'surface-enriched' in rock fragments, curves plotting below are 'depth-enriched'. Pedon sites are listed in order of increasing mean annual precipitation. Dashed lines indicate unimodal distributions, solid lines indicate bimodal distributions. Criteria for determining base of pedon ('bedrock') are described in the text.

fragment modes occur because of mixing from local sources of focused rock fragment production such as bedrock outcrops. While we cannot discount this possibility, the occurrence of rock fragments within nearly all soil horizons (Figure 9), and the dominance of bimodal over unimodal distributions throughout our data set suggest that other explanations may be required.

Implications for sediment supply to rivers

Our findings are potentially useful for modeling the supply of coarse sediment by soil-mantled hillslopes to river networks. For example, in models of river incision into bedrock by mobile sediment (e.g. Sklar and Dietrich, 2004; Lamb *et al.*, 2008), the fraction of the total sediment supply that will move as bedload and the median bedload grain size must be specified. The correlation we observe between F_{RF} and D_{50RF} suggests that these key attributes of sediment supply are not independent, and that knowledge of one could be used to estimate the other. Also, the assumption that bedload sediments are derived from the coarse mode of a bimodal hillslope grain size distribution may simplify modeling of supply and routing of bedload sediments through river networks (e.g. Attal and Lavé, 2006; Sklar *et al.*, 2006) because no knowledge is needed of the size distribution of the sand and finer grain-size supply. Finally, the frequent occurrence of bimodal rock fragment distributions on soil-mantled hillslopes lends support to the hypothesis of Wolcott (1988) that the widely-observed gap in river bed sediments between 1 and 20 mm could be due to bimodal supply by hillslopes, rather than selective transport or particle abrasion within the fluvial system.

Summary and Conclusion

We explored the potential utility of the NRCS soils databases for data mining to document patterns in the abundance and size distribution of rock fragments ($D > 2$ mm) in soils. We focused on data taken from soil pits of the Sierra Nevada of California, the Cascade Mountains of Washington, and two regions of the Hawaiian Islands, where elevation transects span a range of environmental conditions. We filtered the data to select only pedons where database records indicated that pits were dug on hillslopes with active soil production, and not in locations of long-term net soil accumulation. For each of the 27 pedons selected, we constructed depth-averaged grain size distributions and calculated the mass fraction of rock fragments (F_{RF}) and the median rock fragment grain size (D_{50RF}). We also categorized size distributions as unimodal or bimodal, depending on the occurrence of a clear 'breakpoint' between fine and coarse modes.

We find rock fragments in 86% of the pedons examined, with rock fragments occurring primarily in distinct coarse modes within bimodal soil particle size distributions. Rock fragment abundance and median size are strongly correlated, although the scaling between F_{RF} and D_{50RF} differs between the warmer Hawaiian Island sites and the colder Sierra Nevada and Cascade Mountain sites. We also find a contrast between regions in the variation in F_{RF} with elevation, in which F_{RF} declines with elevation in the Hawaiian Island sites, but increases with elevation in the mainland sites. There is a risk that this pattern is an artifact of variation in lithology or erosion rate, however, we speculate that mean annual precipitation may influence this and other patterns we observe in the data. Within each region, higher precipitation rate correlates with lower rock fragment abundance, reduced occurrence of bimodal size distributions, and a shift in the vertical distribution of rock fragments toward deeper portion of the soil column. These empirical observations may be useful in refining models of coarse sediment supply to rivers, and suggest many opportunities for future field investigations, theory development, and additional data mining to refine and test mechanistic hypotheses for the variation in rock fragment size and abundance on soil-mantled hillslopes.

Supporting Information

Supporting information may be found in the online version of this article.

References

Abrahams AD, Parsons AJ. 1994. Hydraulics of interrill overland flow on stone-covered desert surfaces. *Catena* **23**: 111–140.

Attal M, Lavé J. 2006. Changes of bedload characteristics along the Marsyandi River (central Nepal): implications for understanding hillslope sediment supply, sediment load evolution along fluvial networks, and denudation in active orogenic belts. *Special Papers – Geological Society of America* **398**: 143.

Blott SJ, Pye K. 2001. Gradistat: a grain size distribution and statistics package for the analysis of unconsolidated sediments. *Earth Surface Processes and Landforms* **26**: 1237–1248.

Bunte K, Abt SR. 2001. *Sampling Surface and Subsurface Particle-size Distributions in Wadable Gravel- and Cobble-bed Streams for Analyses in Sediment Transport, Hydraulics, and Streambed Monitoring*, General Technical Report No. RMRS-GTR-74. US Department of Agriculture Forest Service: Fort Collins, CO.

Burbank DW. 1991. Late quaternary snowline reconstructions for the southern and central Sierra Nevada, California and a reassessment of the "Recess Peak Glaciation". *Quaternary Research* **36**: 294–306.

Burnett JL, Jennings CW. 1962. *Geologic Map of California: Chico Sheet*, Scale 1:250,000. California Division of Mines and Geology: Sacramento, CA.

Burt R. 2004. *Soil Survey Laboratory Methods Manual*, NSS Laboratory Soil Survey Investigations Report. No. 42. US Department of Agriculture, Natural Resource Conservation Service: Washington, DC.

Casagli N, Ermini L, Rosati G. 2003. Determining grain size distribution of the material composing landslide dams in the Northern Apennines: sampling and processing methods. *Engineering Geology* **69**: 83–97.

Chadwick OA, Gavenda RT, Kelly EF, Ziegler K, Olson CG, Elliott WC, Hendricks DM. 2003. The impact of climate on the biogeochemical functioning of volcanic soils. *Chemical Geology* **202**: 195–223.

Church MA, Mclean DG, Wolcott JF. 1987. River bed gravels: sampling and analysis. In *Sediment Transport in Gravel-bed Rivers*. Thorne CR, Bathurst JC, Hey RD (eds). John Wiley & Sons: New York; 43–88.

Cook RD, Weisber S. 1982. *Residuals and Influence in Regression*. Chapman & Hall: New York.

Crews TE, Kitayama K, Fownes JH, Riley RH, Herbert DA, Muellerdombois D, Vitousek PM. 1995. Changes in soil-phosphorus fractions and ecosystem dynamics across a long chronosequence in Hawaii. *Ecology* **76**: 1407–1424.

Dahlgren R, Boettinger J, Huntington G, Amundson R. 1997. Soil development along an elevational transect in the western Sierra Nevada, California. *Geoderma* **78**: 207–236.

De Vries M. 1970. On the accuracy of bed-material sampling. *Journal of Hydraulic Research* **8**: 523–533.

Fletcher RC, Buss HL, Brantley SL. 2006. A spheroidal weathering model coupling porewater chemistry to soil thicknesses during steady-state denudation. *Earth and Planetary Science Letters* **244**: 444–457.

Graham RC, O'Geen AT. 2010. Soil mineralogy trends in California landscapes. *Geoderma* **154**: 418–437.

Graham R, Rossi A, Hubbert K. 2010. Rock to regolith conversion: producing hospitable substrates for terrestrial ecosystems. *GSA Today* **20**: 4–9.

Granger DE, Riebe CS, Kirchner JW, Finkel JW. 2001. Modulation of erosion on steep granitic slopes, as revealed by cosmogenic ^{26}Al and ^{10}Be. *Earth and Planetary Science Letters* **186**: 269–281.

Hales TC, Roering JJ. 2005. Climate-controlled variations in scree production, Southern Alps, New Zealand. *Geology* **33**: 701–704. DOI. 10.1130/G21528.1

Heimsath AM, Chappell J, Dietrich WE, Nishiizumi K, Finkel RC. 2000. Soil production on a retreating escarpment in southeastern Australia. *Geology* **28**: 787–790.

Heimsath AM, Dietrich WE, Nishiisumi K, Finkel RC. 1997. The soil production function and landscape equilibrium. *Nature* **388**: 358–361.

Heimsath AM, Dietrich WE, Nishiizumi K, Finkel RC. 1999. Cosmogenic nuclides, topography, and the spatial variation of soil depth. *Geomorphology* **27**: 151–172.

Hendricks DM, Whittig LD. 1968. Andesite weathering 1. Mineralogical transformations from andesite to saprolite. *Journal of Soil Science* **19**: 135–146.

Howard AD. 1980. Thresholds in river regimes. In *Thresholds in Geomorphology*, Coates DR, Vitek JD (eds). Allen and Unwin: Winchester, Mass; 227–258.

Hwang SI, Lee KP, Lee DS, Powers SE. 2002. Models for estimating soil particle-size distributions. *Soil Science Society of America Journal* **66**: 1143–1150.

Isherwood D, Street A. 1976. Biotite-induced grussification of the Boulder Creek granodiorite, Boulder County, Colorado. *Bulletin of the Geological Society of America* **87**: 366–370.

Kondolf GM, Wolman MG. 1993. The sizes of salmonid spawning gravels. *Water Resources Research* **29**: 2275–2285.

Lamb MP, Dietrich WE, Sklar LS. 2008. A model for fluvial bedrock incision by impacting suspended and bed load sediment. *Journal of Geophysical Research, Earth Surface* **113**: 03025.

Leopold LB, Wolman MG. 1957. *River Channel Patterns, Braided, Meandering and Straight*, Geological Survey Professional Paper 282–B. US Geological Survey: Washington, DC.

Ludington S, Moring BC, Miller RJ, Stone PA, Bookstrom AA, Bedford DR, Evans JG, Haxel GA, Nutt CJ, Flyn KS. 2007. *Preliminary Integrated Geologic Map Databases for the United States Databases for the United States –- Western States: California, Nevada, Arizona, Washington, Oregon, Idaho, and Utah*, US Geological Survey, Open-File Report OF-2005-1305. Version 1.3, original file updated in December 2007, Scale 1:500,000. http:// pubs.usgs.gov/of/2005/1305/index.htm

Lydon PA, Gay TE Jr, Jennings CW. 1960. *Geologic Map of California, Westwood Sheet*, Scale 1:250,000. California Division of Mines and Geology: Sacramento, CA.

Meyer KA, Griffith JS. 1997. Effects of cobble-boulder substrate configuration on winter residency of juvenile rainbow trout. *North American Journal of Fisheries Management* **17**: 77–84.

Nyssen J, Poesen J, Moeyersons J, Lavrysen E, Haile M, Deckers J. 2002. Spatial distribution of rock fragments in cultivated soils in northern Ethiopia as affected by lateral and vertical displacement processes. *Geomorphology* **43**: 1–16.

Parker G, Wilcock PR, Paola C, Dietrich WE, Pitlick J. 2007. Physical basis for quasi-universal relations describing bank-full hydraulic geometry in single thread gravel-bed rivers. *Journal of Geophysical Research, Earth Surface* **112**: F04005. DOI. 10.1029/2006JF000549

Perfect E. 1997. Fractal models for the fragmentation of rocks and soils: a review. *Engineering Geology* **48**: 185–198.

Phillips JD, Luckow K, Marion DA, Adams KR. 2005. Rock fragment distributions and regolith evolution in the Ouachita Mountains, Arkansas, USA. *Earth Surface Processes and Landforms* **30**: 429–442.

Phillips JD, Marion DA. 2004. Pedological memory in forest soil development. *Forest Ecology and Management* **188**: 363–380.

Poesen J, Lavee H. 1994. Rock fragments in top soils – significance and processes. *Catena* **23**: 1–28.

Poesen JW, Van Wesemael B, Bunte K, Benet AS. 1998. Variation of rock fragment cover and size along semiarid hillslopes: a case-study from southeast Spain. *Geomorphology* **23**: 323–335.

PRISM Climate Group. 2008. Oregon State University. http://www.prismclimate.org

Radoane M, Radoane N, Dumitriu D, Miclaus C. 2008. Downstream variation in bed sediment size along the East Carpathian Rivers: evidence of the role of sediment sources. *Earth Surface Processes and Landforms* **33**: 674–694.

Reasoner MA, Davis PT, Osborn G. 2001. Evaluation of proposed early-Holocene advances of alpine glaciers in the north cascade range, Washington State, USA: constraints provided by palaeoenvironmental reconstructions. *The Holocene* **11**: 607–611.

Reiners PW, Ehlers TA, Mitchell SG, Montgomery DR. 2003. Coupled spatial variations in precipitation and long-term erosion rates across the Washington Cascades. *Nature* **426**: 645–647. DOI. 10.1038/nature02111

Riebe CS, Kirchner JW, Finkel RC. 2004. Erosional and climatic effects on long-term chemical weathering rates in granitic landscapes spanning diverse climate regimes. *Earth and Planetary Science Letters* **224**: 547–562.

Riebe CS, Kirchner JW, Granger DE, Finkel RC. 2000. Erosional equilibrium and disequilibrium in the Sierra Nevada, inferred from cosmogenic ^{26}Al and ^{10}Be in alluvial sediment. *Geology* **28**: 803–806.

Rieke-Zapp D, Poesen J, Nearing M. 2007. Effects of rock fragments incorporated in the soil matrix on concentrated flow hydraulics and erosion. *Earth Surface Processes and Landforms* **32**: 1063–1076. DOI. 10.1002/esp.1469

Roering J, Almond P, Tonkin P, Mckean J. 2002. Soil transport driven by biological processes over millennial time scales. *Geology* **30**: 1115–1118.

Schuur EAG, Chadwick OA, Matson PA. 2001. Carbon cycling and soil carbon storage in mesic to wet Hawaiian montane forests. *Ecology* **82**: 3182–3196.

Sharmeen S, Willgoose GR. 2007. A one-dimensional model for simulating armouring and erosion on hillslopes: 2. Long term erosion and armouring predictions for two contrasting mine spoils. *Earth Surface Processes and Landforms* **32**: 1437–1453.

Sherrod DR, Sinton JM, Watkins SE, Brunt KM. 2007. *Geologic Map of the State of Hawai'I*, US Geological Survey Open-File Report 2007–1089, 83 pp., 8 plates, Scales 1:100,000 and 1:250,000, with GIS database. US Geological Survey: Reston, VA.

Shirazi MA, Boersma L. 1984. A unifying quantitative analysis of soil texture. *Soil Science Society of America Journal* **48**: 142.

Simanton JR, Renard KG, Christiansen CM, Lane LJ. 1994. Spatial-distribution of surface rock fragments along catenas in semiarid Arizona and Nevada, USA. *Catena* **23**: 29–42.

Sklar LS, Dietrich WE. 2004. A mechanistic model for river incision into bedrock by saltating bed load. *Water Resources Research* **40**: W06301.

Sklar LS, Dietrich WE. 2006. The role of sediment in controlling steady-state bedrock channel slope: implications of the saltation–abrasion incision model. *Geomorphology* **82**: 58–83.

Sklar LS, Dietrich WE, Foufoula-Georgiou E, Lashermes B, Bellugi D. 2006. Do gravel bed river size distributions record channel network structure? *Water Resources Research* **42**: W06D18.

Smith GHS, Nicholas AP, Ferguson RI. 1997. Measuring and defining bimodal sediments: problems and implications. *Water Resources Research* **33**: 1179–1185.

Soil Survey Division Staff. 1993. *Soil Survey Manual, Soil Conservation Service*, Handbook 18. US Department of Agriculture: Washington, DC.

Soil Survey Staff. 2006. *Keys to Soil Taxonomy*, 10th ed. US Department of Agriculture-Natural Resources Conservation Service: Washington, DC.

Soil Survey Staff. 2008. *National Soil Survey Characterization Data*. Soil Survey Laboratory, National Soil Survey Center, USDA-NRCS: Lincoln, NE. http://ssldata.nrcs.usda.gov/default.htm

Sun D, Bloemendal J, Rea DK, Vandenberghe J, Jiang F, An Z, Su R. 2002. Grain-size distribution function of polymodal sediments in hydraulic and aeolian environments, and numerical partitioning of the sedimentary components. *Sedimentary Geology* **152**: 263–277.

Tabor R, Frizzell V, Whetten J, Waitt R, Swanson D, Byerly G, Booth D, Hetherington M, Zartman R. 1987. *Geologic Map of the Chelan 30-minute by 60-minute Quadrangle, with Accompanying Report*. US Geological Survey, Miscellaneous Investigations Series Map I-1661, Scale 1:100000. US Geological Survey: Reston, VA.

US Department of Agriculture, Natural Resource Conservation Service (USDA NRCS). 2005. *Soil Survey Laboratory Information Manual*, Soil survey investigations report number 45. Version 1.0: May 1995. ftp://ftp-fc.sc.egov.usda.gov/NSSC/Lab_Info_Manual/ssir45.pdf

US Department of Agriculture, Natural Resource Conservation Service (USDA NRCS). 2007. National Soil Survey Handbook, Title 430-VI. http://soils.usda.gov/technical/handbook/

US Department of Agriculture, Natural Resource Conservation Service (USDA NRCS). 2011. Soil Survey Staff. Official Soil Series Descriptions. http://soils.usda.gov/technical/classification/osd/index.html

Vitousek PM. 2004. *Nutrient Cycling and Limitation: Hawai'i as a Model System*. Princeton University Press: Princeton, NJ.

Vitousek P, Chadwick O, Matson P, Allison S, Derry L, Kettley L, Luers A, Mecking E, Monastra V, Porder S. 2003. Erosion and the rejuvenation of weathering-derived nutrient supply in an old tropical landscape. *Ecosystems* **6**: 762–772. DOI. 10.1007/ s10021-003-0199-8

Vitousek PM, Chadwick OA, Crews TE, Fownes JH, Hendricks DM, Herbert D. 1997. Soil and ecosystem development across the Hawaiian islands. *GSA Today* **7**: 1–8.

Wahrhaftig C. 1965. Stepped topography of the southern Sierra Nevada, California. *Geological Society of America Bulletin* **76**: 1165.

Wakabayashi J, Sawyer TL. 2001. Stream incision, tectonics, uplift, and evolution of topography of the Sierra Nevada, California. *Journal of Geology* **109**: 539–562.

West AJ, Galy A, Bickle M. 2005. Tectonic and climatic controls on silicate weathering. *Earth and Planetary Science Letters* **235**: 211–228.

Whipple K. 2004. Bedrock rivers and the geomorphology of active orogens. *Annual Review of Earth and Planetary Sciences* **32**: 151–185. DOI. 10.1146/annurev.earth.32.101802.120356

White A, Brantley S. 2003. The effect of time on the weathering of silicate minerals: why do weathering rates differ in the laboratory and field? *Chemical Geology* **202**: 479–506. DOI. 10.1016/j.chemgeo.2003.03.001

Wilcock PR. 1993. Critical shear stress of natural sediments. *Journal of Hydraulic Engineering* **119**: 491–505.

Wolcott J. 1988. Nonfluial control of bimodal grain-size distributions in river-bed gravels. *Journal of Sedimentary Research* **58**: 979–984.

Wolfe EW, Morris J. 1996. *Geologic Map of the Island of Hawaii*. Miscellaneous Investigations Series Map I-2524-A. US Geological Survey: Reston, VA.

Yoo K, Amundson R, Heimsath AM, Dietrich WE, Brimhall GH. 2007. Integration of geochemical mass balance with sediment transport to calculate rates of soil chemical weathering and transport on hillslopes. *Journal of Geophysical Research* **112**: F02013. DOI. 10.1029/2005JF000402

Yoo K, Mudd S. 2008. Discrepancy between mineral residence time and soil age: implications for the interpretation of chemical weathering rates. *Geology* **36**: 35–39.